POWDER DIFFRACTION

CAMBRIDGE UNIVERSITY PRESS

Rietveld Texture Analysis from Synchrotron Diffraction Images: II. Complex multiphase materials and diamond anvil cell experiments

Journal:	*Powder Diffraction*
Manuscript ID:	PD-CE-2013-0002
Manuscript Type:	Crystallography Education
Date Submitted by the Author:	01-Mar-2013
Complete List of Authors:	Wenk, Hans-Rudolf; University of California, EPS Lutterotti, Luca; University of Trento Kaercher, Pamela; University of California, Earth and Planetary Science Kanitpanyacharoen, Waruntorn; University of California, Earth and Planetary Science Miyagi, Lowell; University of Utah, Geology an d Geophysics Vasin, Roman; University of California, Earth and Planetary Science
Keywords:	Texture analysis, Synchrotron diffraction, Rietveld method, Shale, Diamond anvil cell

Rietveld Texture Analysis from Synchrotron Diffraction Images: II. Complex multiphase materials and diamond anvil cell experiments

Hans-Rudolf Wenk[1)], Luca Lutterotti[2)], Pamela Kaercher[1)], Waruntorn Kanitpanyacharoen[1)], Lowell Miyagi[3)], Roman Vasin[1,4)]

Department of Earth and Planetary Science, University of California, Berkeley, CA
Department of Industrial Engineering, University of Trento, Italy
Department of Geology and Geophysics, University of Utah, Salt Lake City
Frank Laboratory of Neutron Physics, Joint Institute for Nuclear Research, Dubna, Russia

Abstract

Synchrotron X-ray diffraction images are increasingly used to characterize crystallographic preferred orientation distributions (texture) of fine-grained polyphase materials. Diffraction images can be analyzed quantitatively with the Rietveld method as implemented in the software package MAUD (Materials Analysis Using Diffraction). Here we describe the analysis procedure for diffraction images collected with high energy X-rays for a complex, multiphase shale, and for those collected *in situ* in diamond anvil cells at high pressure and anisotropic stress.

Key words: Texture analysis, Synchrotron diffraction, Rietveld method, Shale, Diamond anvil cell

I. INTRODUCTION

In a companion paper (Wenk *et al*., 2013), we have described the basic steps for texture analysis from synchrotron diffraction images with the Rietveld method, using the software MAUD (Lutterotti *et al*., 1997). We assume that the reader is familiar with the procedure. We will refer to some of the steps used for the general procedure from the companion paper with the corresponding number (e.g., **Part I.3**). Steps in this publication will be referred to only by number (e.g., **3**). Here we discuss complexities which arise for samples with many phases and samples which are highly deformed.

The first example is a sedimentary shale composed of multiple types of minerals, with different volume fractions, microstructures, and orientation distribution functions (ODFs). The second complex sample is magnesiowuestite (Mg,Fe)O measured *in situ* at ultrahigh pressure and anisotropic stress conditions with a diamond anvil cell (DAC). Keep in mind that we provide only an outline of analysis procedures. The Rietveld method and its implementation in MAUD is very general and lends itself to many applications, each of which may require slightly different approaches, modifications, and application of particular models. Data files for this tutorial can be freely downloaded from the internet (http://eps.berkeley.edu/~wenk/TexturePage/MAUD.htm).

II. SHALE AS AN EXAMPLE OF A COMPLEX POLYPHASE MATERIAL

A. Diffraction experiment

Shale is a sedimentary rock composed of many minerals. Sheet silicates comprise a large volume fraction of shales and align preferentially parallel to the bedding plane during sedimentation and compaction. Crystallographic preferred orientation (CPO) of phyllosilicates is of great interest, because it is the primary cause of elastic anisotropy observed during seismic prospecting of oil and gas deposits. Thus several studies have focused on improving synchrotron X-ray techniques to quantify textures and microstructures of shales (*e.g.*, Wenk *et al.*, 2008; Lutterotti *et al.*, 2010; Kanitpanyacharoen *et al.*, 2011, 2012; Vasin *et al*., 2013).

For this tutorial we use a sample of Kimmeridge shale from the North Sea, UK (Hornby, 1998; Wenk *et al.,*2010; Vasin *et al*., 2013). The sample is a slab, 2mm thick (Fig. 1a). It was measured at the APS high energy beamline ID-11C during the same session as the nickel coin (Wenk *et al.*, 2013). The wavelength is 0.10798 Å, and the beam size 0.5×0.5 mm. Therefore the same instrument parameters can be applied which were obtained by refining the CeO_2 standard

(see **Part I.1-13**). During X-ray exposure, the sample was translated along the horizontal axis from –2.5 to +2.5 mm to increase the measured volume and rotated around the ω-axis (Fig. 1 in Wenk *et al.*, 2013) from –45° to +45° in 15° increments (i.e., there are 7 diffraction images) to obtain adequate pole figure coverage.

Images were collected with a Perkin Elmer amorphous silicon detector with dimensions of 2048×2048 pixels and a pixel size of 200×200 μm. The detector was approximately 1850 mm from the sample. Figure 2a shows a diffraction image with many Debye-rings from at least six major phases. Several rings display strong intensity variations due to preferred orientation.

B. Analysis for axial symmetry

1. *Start.* Open a new analysis in MAUD ("File → New → General Analysis") and save it ("File → Save analysis as…") in your data directory (*e.g.* as Shale2012-axial.par). Refining seven datasets (2D diffraction images are integrated in 10° steps, resulting a total of 36x7 = 252 spectra) simultaneously with a number of low-symmetry phases is time-consuming. Thus we will start with only one dataset measured at ω = 0°. The procedure with a single image is justified, because shale textures have approximately axial (cylindrical) symmetry about the bedding plane normal. By imposing this sample symmetry, complete pole figure coverage is obtained with only one dataset.

2. *Datasets*.

- *General*: Import calibrated diffractometer parameters (CeO2-2012.ins) as was done for the coin analysis (**Part I.15**). Restrict the refinement range to 2θ = 0.3 – 3.0° (**Part I.8**). Since this shale contains several low-symmetry phases, many peaks lie at higher 2θ due to higher order reflections that strongly overlap. They do not provide much information for texture analysis, and restricting the range will greatly speed up the computation.
- *Datafiles*: Import the diffraction image (**Part I.5-7**). In ImageJ plugin, load Hornby-long-00132-0.tif, then proceed with the same steps and values as for the CeO_2 standard and nickel coin (**Part I.5-7**, **Part I.15**) (*i.e.* for image width/height size 2048×2048, pixel size 0.2×0.2 mm, detector distance 1850 mm, image rotation "rotate 90 degrees left to correctly account for your sample rotation axis, etc.). Save the .esg file (*e.g.*, as "Hornby-long-00132-0.esg") in your data directory, and close ImageJ. As a reminder: Images need

to be rotated 90° left in ImageJ similarly to CeO_2 and nickel coin (**Part I.5**). In Figure 3 (bottom) the stack of experimental diffraction spectra is displayed. The pole figure coverage is shown in Figure 1b with the pole to the bedding plane at A (ω rotation axis).

- *Background function:*
    - *Polynomial*–We will use a 4th order polynomial background common to all patterns. By default, MAUD provides three polynomial background coefficients, and two additional coefficients need to be added in the "DataFileSet" window under "Background function" tab in "Polynomial" (**Part I.8**). Right-click on each of the five background parameter values, and set them to "Refined".
    - *Background peaks*–It is necessary to correct for small angle scattering from platelet-shaped phyllosilicate nanoparticles, which is best visible in the diffraction image (Fig. 2a) at very low angles (2θ ≈ 0.1-0.2°) close to the beamstop. Since these platelets are oriented also small angle scattering displays azimuthal intensity variations. The broad peak extends as elevated background to the first diffraction peaks of phyllosilicates (2θ ≈ 0.6°) (Fig. 3). To correct for it, we add two symmetrical background peaks. In "Background function" go to "Background peaks" and click "Add term" (Fig. 4). The first peak is assumed to have an intensity ("Height") of 100,000, width in 2θ "HWHM" equal to 0.1°, width in eta ("HWHW (eta)") of 30°, position along 2θ ("Position") of 0.1°, position along azimuth ("Position (eta)") of 90°. Also set "Eta" = 1, and "Eta (eta)" = 0.5. These parameters control gaussianity of background peaks in 2θ and eta domains. Use the same parameters for the second peak, but change its "Position (eta)" to 270°. Double-click on background peak names to rename them. Right click on the "Height", "HWHM" and "HWHM (eta)" boxes of both background peaks and choose the "Refined" option.
- *Save*: Make sure to save the parameter file with .par extension and in the same folder as the .esg data files.

3. *Phases.* To reduce the refinement time in this tutorial we limit our refinement to the five major phases: quartz, pyrite, kaolinite, illite-mica, and illite-smectite. There are minor phases such as feldspars with less than 5% volume and no significant texture. Quartz and pyrite structures are included in structures.mdb file of MAUD (**Part I.16**). We provide crystallographic information files (.cif) for triclinic kaolinite (Bish and Von Dreele, 1989), monoclinic illite-mica (Gualtieri, 2000), and monoclinic illite-smectite (Plançon *et al.*, 1985). Refer to sections **Part I.2**, **I.9**, and **I.16** for information on importing .cif and working with phases. For illite-mica and illite-smectite, the first monoclinic setting has to be used (Matthies and Wenk, 2009). The provided .cif file for illite-smectite is already in the first setting. But you do need to "Edit" the illite-mica phase and under "General" change the space group from C2/c:b1 to C2/c:c1, which makes *c* the unique (2-fold) axis. Lattice parameters and atomic positions are adjusted automatically by MAUD. Rename the displays of mineral phases by double-clicking on their names.

4. *Sample.* When multiple phases are entered, MAUD automatically assigns to each phase the same volume fraction. But with a complex sample like this shale, it is better to provide good initial estimates of phase volume fractions. Switch to "Sample" tab in the MAUD main window and "Edit" current sample. In "Layers" pick a phase from drop-down list in the right part of the window and enter a new value in the "Volume fraction" field. We start with 0.25 for quartz, 0.05 for pyrite, 0.1 for kaolinite, 0.3 for illite-mica and 0.3 for illite-smectite. Weight fractions are calculated automatically by MAUD using the provided atomic structure.

Also, to correctly impose axial symmetry for texture, the sample orientation in the MAUD reference coordinate system must be changed. Go to "Sample position" and set the Chi value to 90°. This puts the bedding plane normal of the shale into the center of the reference pole figure (B in Fig. 1b). Axial symmetry of texture in MAUD is always imposed around this axis.

5. *Manual adjustments.* Manual adjustments of parameters are best done in "Parameter list" ("Analysis → Parameters list" or "Ctrl" and "L" on a PC or "Command" and "L" on a Mac), expanding parameters, clicking on "Value" and selecting increment to decrease or increase the value by clicking on arrows. Results are automatically updated on the "Plot" display (**Part I.12**).

- Start by pressing the "Calculator" button in the MAUD main window toolbar to view calculated spectra. At the bottom of the "Plot" display there appears a list of phases with

each phase name of different color (unless "Black & White" is selected in "Plot options") (Fig. 5). For each phase positions of diffraction peaks are displayed. By right-clicking on the phase name in this list, and selecting one or several phases from the menu, individual contributions of selected phases are plotted with corresponding colors.

- You may need to adjust some of the phase lattice parameters manually to shift position to a reasonable value. For this example, the overall calculated intensity is too low, and has to be adjusted manually to roughly match the experiment (**Part I.18**). Save your analysis before beginning refinements.

6. *Basic refinement.* The sample is too complex to use the Wizard, and we will proceed with a mixture of semi-automatic refinement and manual (similar to **Part I.10-12**). Free and refine the parameters in the order listed below but first (in "Parameter list") "Fix all parameters". Then refine each parameter or parameter group until the fit has converged or is no longer visibly improving, then move on to the next parameter (usually, 4-6 iterations are enough). After you have refined a parameter, leave it free to refine, as you free and refine the next parameter in the list. If your refinement diverges, you may have to intervene with manual adjustments to bring the diverging parameters into a reasonable range. It is advised to save your analysis after each successful refinement (preferably to separate files, so that you can backtrack in case the refinement diverges and requires manual adjustments).

- *Intensity and backgrounds*. In "Parameter list", click "Free scale pars". This will set to "Refined" the overall scale of the diffraction pattern and the phase volume fractions (except the first one that is adjusted each cycle so that volume fractions add to 1). We have already set manually all five polynomial background coefficients and background peak intensity and width to "Refined" (**2**). Refrain from clicking the "Free backgrounds" button as this would refine all background peaks parameters, including positions that are fixed.
- *Thermal factors*. These diffraction data are not appropriate to refine thermal factors separately for each atom type, thus set them all equal. Click the "Bound B factors" button in the parameter list. This sets all thermal factors equal to the B factor of the first atom of the first phase in the list and sets this one to "Refined." Run the refinement again. For these diffraction data with a narrow scattering angle range the refinement of the B-factors

is used as a 2θ dependent intensity adjustment, only remotely related to physical thermal vibrations.

- *Cell parameters*. All cell parameters for quartz (*a* and *c*) and pyrite (*a*) are refined since these minerals contribute several distinct sharp peaks to the diffraction pattern. Phyllosilicate peaks are weaker and strongly overlapped; thus for kaolinite and illite-mica we will not refine cell angles, but only *a*, *b* and *c*. For illite-smectite, refine only the *a* parameter. MAUD offers a user-friendly approach for the refinement of these parameters. While in "Parameters list" enter the word "cell" into a search field at the bottom. This will make only cell parameters of all phases in the sample visible in the parameters list and you may quickly set up their "Refined" status without extensive browsing.
- Make sure that you have refined the parameters specified above. Compare experiment and model on "Plot" and "Plot 2D" displays, check that all phase volume fractions are reasonable (*e.g.*, no phases have 0% volume fraction) and that cell parameters did not change significantly from their initial values.
- *Detector position.* Because the shale sample is not in the exact same position as the CeO_2 calibrant, the detector orientation relative to the sample is slightly different and should be refined. Set "Center displacement x," Center displacement y," "Tilting error x," and "Tilting error y" (in "Datasets → Diffraction Instrument → Flat Image Transmission") to refine. Close all windows and run the refinement. When the refinement is done, set these four parameters back to "Fixed."

7. *Texture and microstructure refinement.* In the "Plot 2D" display (Fig. 3), diffraction peaks of kaolinite, illite-mica, and illite-smectite show strong eta-dependent intensity variations indicative of texture. The intensities of the quartz and pyrite diffraction peaks are almost constant, except for several increased intensity spots due to scattering from larger grains. Thus we will only refine preferred orientations of the three phyllosilicates but not of quartz and pyrite. Note that some of the peaks have incorrect width. We need to refine microstructure parameters of phases to correct this. To setup the texture and microstructure refinement, proceed with the following steps.

- Select kaolinite, edit the phase and in the "Microstructure" tab, ensure that the "Delf" line broadening model and the "Isotropic" size strain models are selected (see section VII in Wenk *et al.*, 2013, for details and references). Click the "Options" button next to "Size-

Strain model/Isotropic," and in the new window, set both parameters (crystallite size and r.m.s. microstrain) to "Refined".

- Go to "Advanced models", and select the E-WIMV model for texture (**Part I.16**). Click on the corresponding "Options" button. In the "E-WIMV options panel" select 10 iterations and a 10° for "ODF resolution in degrees". For "Generate symmetry" select "cylindrical". Phyllosilicates in shale display almost perfect fiber texture, thus imposing axial symmetry is justified. To speed up the refinement, click "EWIMV advanced options" button. In "Min reflex intensity" enter 0.01. It means that all the diffraction peaks with intensity below 1% of maximum peak intensity for this phase will not be used for texture calculation. Close all windows ("OK") to save changes and return to MAUD main window. Repeat this procedure for illite-mica.
- For illite-smectite, with a highly disordered structure, we will use the "Standard Functions" for texture model and an appropriate stacking disorder model. The so-called "Ufer single layer" model uses a super-cell approximation (Ufer *et al.*, 2004), and consequently the number of peaks fitting the pattern is increased by at least one order of magnitude. Due to an increased number of peaks and peak overlaps, the E-WIMV algorithm will run very slowly, and errors are possible when resolving diffraction peak overlaps. Thus the standard functions texture model is more appropriate in this case.
- "Edit" the illite-smectite phase, and proceed to the "Advanced models" tab then select "Standard functions" as a texture model. Click the "Options" button. In window "Texture options panel" click the "Add term" button in the "Fiber components" panel, and set "ODF background" = 0, "Intensity" = 0.7, "ThetaY" = 0, "PhiY" = 0 (fiber axis is normal to the conventional pole figure projection plane in MAUD), "ThetaH" = 90, "PhiH" = 0 (fiber axis is parallel to *a* translation), "FWHM" = 30, and "Gaussian" = 0.5. Set "Intensity", "FWHM" and "Gaussian" values to "Refined", then click "OK".
- Go to the "Microstructure" tab of the phase options window. Click the "Options" button next to "Size-Strain model/Isotropic," and in the new window change crystallite size to 200 and r.m.s. microstrain to 0.01. Set both to "Refined". Then select "Ufer single layer" as the "Planar defects model" and click "Options" button. In window "Single layer model options panel" set "Number of layers" = 10, "Stacking direction" = a, "Crystallite factor" = 1 (< 1 will produce additional peak broadening to (h00) type peaks), and "Microstrain

factor" = 1 (> 1 will produce additional peak broadening to (h00) type peaks). Refine "Crystallite factor" and "Microstrain factor".

- Leave crystallite size and r.m.s. microstrain at the default values (1000 Å and $8E10^{-4}$, correspondingly) for quartz and pyrite and set these to "Refined".
- Run the refinement. At the end of the refinement, the experimental and the calculated spectra should agree fairly well in the "Plot" (Fig. 5) and "Plot 2D" (Fig. 3) displays. There are deviations in relative intensities in the "Plot" display, because this is simply an average over all spectra, not considering the relative significance of the orientation distribution. Figure 5 compares two individual spectra (obtained in "Datasets →Datafiles →View"), one with scattering vectors parallel and one perpendicular to the bedding plane normal and a good agreement for both is observed. Table 1 lists refined volume and weight fractions for the phases.

8. *Plot pole figures.* Go to the "Graphic → Texture plot" menu to view "Reconstructed intensity" of the pole figures(**Part I.20**). Select the "Active" boxes next to (001) for kaolinite (phase is chosen from "Phase" drop-down menu), and (200) for illite-mica and illite-smectite. Since we have imposed fiber symmetry, the pole figures are circular around the center with the maximum for the basal plane poles in the center (normal to bedding plane). In the "E-WIMV" window we have exported ODF's of kaolinite and illite-mica in BEARTEX format (Wenk *et al.*, 1998), then smoothed in BEARTEX with a 7.5° Gaussian filter and calculated pole figures. In the "Standard function" window we have also exported pole figures for illite-smectite. The pole figures are shown in Figure 6a in equal area projection. Note that illite-mica has the sharpest texture and illite-smectite shows the broadest distribution. Some data are summarized in Table 2. Save the parameter file.

C. Analysis without imposing texture symmetry

9. As a last step, we add the other six diffraction images to the analysis. We save the refinement which we just did under a different name (*e.g.* as Shale2012-nosymm.par).

- We create a new dataset by duplicating the available set ("Edit → Duplicate object") and "Edit" the copy by removing in "Datafiles" all datafiles in the list (select them all and click "Remove"), and then duplicate this new 'empty' dataset five more times.

- Load corresponding datafiles into the six new datasets following the procedure in **Part I.5-8**. Change the corresponding omega angles for each image (in "Datafiles → Modify Angles", **Part I.15**). Rename the new datasets in the main MAUD window (*e.g.*, assign corresponding omege angle values as their names). The pole figure coverage is now as shown in Figure 1c, but considering the 90° Chi rotation (**4**), is shown in Figure 1d. Save the parameter file.
- Compute the model spectra, and review them in the "Plot" and "Plot 2D" displays. The calculated and experimental diffraction spectra should agree fairly well. Since all necessary phase parameters already have good starting values and are set to refine, there are only a few things that we need to adjust before final refinement.
- Go to "Parameter list" ("Analysis→Parameters list" menu) and click "Free scale pars" to refine incident intensity values for datasets we just added. Second, change the texure function of illite-smectite from "Standard Function" to "E-WIMV". For each of the phyllosilicate phases, go to "E-WIMV options panel" (see **7** and **Part I.8**) and change option under "Generate symmetry" to "none". We now have enough data to proceed without ODF symmetry imposed.
- Refine your data.

Pole figures of phyllosilicates, corresponding to those in Figures 6a but without imposing symmetry, are shown in Figure 6b. The pole figure coverage (Fig. 1d) indicates that during data collection the sample has been rotated around the center. The new pole figures show deviations from axial symmetry, particularly an elongation of the pole figure maximum in the vertical direction for (001) kaolinite as well as (100) illite-mica and illite-smectite. Comparing this with the coverage, we note that this distortion extends into the blind region and may be an artifact. This is further supported by the fact that maximum pole densities are higher if axial symmetry is imposed (Table 2). Only additional measurements with rotations around the other sample axes could verify if the preferred orientation pattern has perfect axial symmetry. In Figure 7 we also show pole figures (100) of kaolinite and (010) of illite-mica and illite-smectite that display a peripheral circle. Phase volume fractions for Kimmeridge shale without imposing sample symmetry are compared in Table 1 with results for axial symmetry. They are very similar.

11. For the Kimmeridge shale the final R_w factor is ≈ 15% and R_b is ≈ 10%. A few peaks are missing from the calculated diffraction pattern, some are too intense, and some have wrong shapes (*e.g.*, Figs. 3, 5). The missing peaks are mostly due to feldspar that could be entered into the refinement. Anisotropic crystallite shapes and microstrains could also be imposed for phyllosilicates (**Part I.7**). We have used CeO_2 powder to refine instrumental parameters (Wenk *et al.*, 2013), but cerium oxide has no diffraction peaks at $2\theta < 2°$. Thus the function describing instrumental part of diffraction peak broadening (especially the asymmetry) is poorly suited for this shale with diffraction peaks down to $2\theta \approx 0.5°$. Parts of the instrumental peak shape function (Caglioti parameters) can be refined in this example.

III. DIAMOND ANVIL CELL IN RADIAL DIFFRACTION GEOMETRY

A. Experiment

Rietveld texture analysis of synchrotron diffraction images can be applied to study *in situ* deformation at high pressures with a diamond anvil cell in radial diffraction geometry (rDAC) (*e.g.*, Wenk *et al*., 2006). This proves to be an important method to determine deformation mechanisms at ultrahigh pressures, as in the deep earth (*e.g.*, Miyagi *et al*. 2010) to explain observed seismic anisotropy in the lower mantle and inner core, and to study crystal orientation changes during phase transformations (Miyagi *et al*., 2008; Kanitpanyacharoen *et al*., 2012b). The method can also be applied to analysis data from multi-anvil experiments such as D-DIA (*e.g.*, Wenk *et al*., 2005).

The geometry of a typical rDAC deformation experiment is shown in Figure 8a,b. Diamonds not only impose pressure but also differential stress that deforms crystals in the aggregate. The diamond cell is set up in radial rather than axial geometry, i.e. the X-ray beam passes through the sample perpendicular to the compression direction so that the diffraction image records reflections from lattice planes oriented parallel and perpendicular to compression (Fig. 2c). Preferred orientation is expressed in the azimuthal intensity variations, similar to the images of the shale (Fig. 2a).

rDAC experiments have been performed at room temperature to pressures as high as 200 GPa on iron (Wenk *et al*., 2000) and 185 GPa on $MgSiO_3$ post-perovskite (Miyagi *et al*., 2010). More recently texture measurements have been made in the rDAC on magnesiowuestite

(Mg,Fe)O at 2273 K and ≈ 65 GPa, using a combination of resistive and laser heating (Miyagi *et al*., 2013).

Contrary to the coin and shale experiments, we must take into account changes with pressure, and particularly the macroscopic stress field which imposes anisotropic elastic distortions of the lattice. As an example we use magnesiowuestite which has been previously investigated with rDAC experiments (*e.g.*, Merkel *et al*. 2002; Kunz *et al*., 2007; Lin *et al*., 2009; Kaercher *et al*., 2012). This particular sample $(Mg_{0.9}Fe_{0.1})O$ has been described by Marquardt *et al*. (2009) and Miyagi *et al*. (2013).

The rDAC experiment was performed at the high pressure beamline 12.2.2. of the Advanced Light Source in Berkeley. Magnesiowuestite powder was loaded into a boron-kapton gasket. The initial sample diameter was 80 μm with a starting thickness of 50 μm. The sample was compressed in an rDAC, using diamond anvils with 300 μm diameter culets (Fig. 8c). Diffraction images were recorded with a Mar3450 image plate detector, with dimensions of 3450×3450 and a pixel size of 100×100 μm, positioned approximately 285 mm from the sample and an X-ray wavelength of 0.49594 Å.

There are two immediate complications. First, the beam passes not just through the sample but also through a gasket, which is needed to maintain pressure. Thus there are additional diffraction lines from the gasket material, especially at low angles (Fig. 2c). Gaskets for radial DAC experiments must be made of materials that scatter as little as possible. At lower pressures, amorphous boron (< 100 GPa) has been used, while at higher pressure, cubic boron nitride or beryllium have been used. For beryllium which scatters more, it is advantageous to tilt the cell slightly to have minimum beam interference. Bright diffraction spots from the diamond may also appear in the diffraction pattern. In fact, the large spot on the right side of Fig. 2c is attributed to diamond. This effect can be minimized by slightly rotating or tilting the DAC. If the cell is tilted significantly, the tilt needs to be accounted for in the analysis (Merkel, 2006). This is done by entering the appropriate sample rotation angles in MAUD.

A second complication is imposed anisotropic elastic strain. Lattice plane spacings are smaller in the compression direction and larger perpendicular to the compression axis. Thus, the Debye rings are not circles but ellipses. The resulting sinusoidal variations od diffraction peak positions with azimuthal angle are best seen in unrolled images (Fig. 9a, bottom).

B. Initial setup

12. *Instrument calibration.* Before analyzing the MgFeO diffraction pattern, instrument parameters should be refined with a standard sample. In this case LaB_6 is used (Lab6_001.mar3450). Start a new general analysis file, and save it as "LaB6-2012.par". The diffraction image (Fig. 2b) is quite spotty, indicative of large grain size which is not ideal, especially for refining Caglioti parameters. Before using Mar images in MAUD, they have to be converted to 16 bit TIFF images. This can be done in Fit2D (Hammersley, 1998; be aware that sometimes coordinate axis could be inverted or intensities and image size adjusted when doing image conversion with Fit2D) or preferably with the marcvt utility distributed by MarResearch.

Latest versions of marcvt for Linux, MacOS and Windows are freely available at http://www.marresearch.com/download.html. Running marcvt in Microsoft Windows systems requires Cygwin (http://www.cygwin.com/) with libjpeg7 and libpng12 packages. During installation of Cygwin, when prompted to select packages for the installation, uncheck "Hide obsolete packages" box. Afterwards, search for libpng12 (in All/_obsolete subfolder) and libjpeg7 (in All/Graphics subfolder). After setting libpng12 and libjpeg7 for installation, press "Next" button and Cygwin will be installed on your computer. Put the marcvt.exe program into the "bin" subfolder of the Cygwin installation folder. You must also have Administrator rights when opening the Cygwin console and running the marcvt application.

After you made the appropriate .tiff image, proceed with instrumental setup in MAUD (see **Part I.1,4-13** for details). Follow directions in **Part I.1** but enter 0.49594 Å for wavelength and 285 mm as sample-detector distance. Follow step **Part I.5** and load the LaB6 TIFF image. In ImageJ specify correct Mar3450 image plate detector size (3450×3450 pixels) and pixel size (0.1×0.1 mm). Also, do not apply the image rotation ("Image→Rotate→Rotate 90 Degrees Left") in ImageJ. We have only one diffraction image of magnesiowuestite, thus we do not need the image reorientation that was necessary to correctly account for the orientation of the horizontal sample rotation axis for beamline 11-ID-C, described for nickel coin (**Part I.5**, **Part I.15)** and shale (**2**).

Proceed with with **Part I.6**. The image is not well-centered, and you must manually specify estimated detector center coordinates to avoid major distortions of peak positions on different integrated spectra. You will find a reasonable alignment by setting "Center X (mm)" = 172.9 and "Center Y (mm)" = 154.9. Integrate image in 5° sectors ("Number of spectra" = 72). A

reasonable 2θ range for the refinement is 6.0-23.5° For "Background function" we use "Polynomial" with five parameters (**Part I.8**).

Add a LaB_6 phase as described in **PartI.9**. The NIST-recommended cell parameter for LaB_6 is a = 4.15689 Å, crystallite size is 7000 Å, and microstrains are close to zero (set to 1.0E-5).

When you calculate spectra with these parameters, you will notice in the "Plot" display of the MAUD main window additional peaks at 2θ ≈ 8.5°, 13.5°, 17.5° and 20.7° due to some sample contamination. "Edit" current dataset, go to the "Excluded regions" tab and click "add term" button. One excluded region will appear in the list. Input values for "Min in data units" and "Max in data units" (2θ). We recommend excluding regions 2θ ≈ 7.5-9°, 10.5-14.5°, 17.2-19°, 20-21.3°. This is an example of how to exclude "undesirable" data from the refinement. Note that it also excludes a couple of LaB_6 peaks, overlapped with the contamination.

In the "Plot 2D" display, experimental diffraction peaks are hardly visible because of few very intense "spots" originating from diffraction from a few very large grains. To deal with this we select "arbitrary tex" as "Texture model" for LaB_6 (**Part I.9**). In general it would be advisable not to use such a coarse-grained impure standard (Fig. 2b).

For the refinement of instrument parameters proceed like it is described in **Part I.11-12**. In this case you should not refine "Asymmetry" parameters as the measured diffraction peaks are far from image center and thus do not show any broadening asymmetry. Also in this case there is no eta angle dependent broadening. Repeat the refinement until convergence. Save instrument parameters as LaB6-2012.ins (**Part I.13**).

13. Start analysis for the magnesiowuestite DAC image. First, import the instrument parameters which you have just refined (LaB6-2012.ins). Next, convert the diffraction image of magnesiowuestite (MgFeO_25keV_Z3_004.mar3450) into .tiff format (**11**), and import it into MAUD following the same procedure as you just did for LaB_6. Unlike the coin and the shale samples, here you have only one diffraction image. Integrate it in 5° sectors to make 72 .esg files with individual spectra (in ImageJ). This smaller integration step is essential in this case, because there is a sharp texture and significant peak shifts due to anisotropic stress. If the integration step is too large, the variations of diffraction peak positions and intensities can not be accounted for properly. Note when the red (tracker) circle is superposed in ImageJ that the diffraction rings are

not circles but ellipses. They are elongated in the vertical direction (compression direction in the DAC). Also, the sides of the round image are cut by straight shadows originating from the rDAC cell. Do not forget to select the same image center as for the LaB_6 standard when in ImageJ ("Center X (mm)" = 172.9 and "Center Y (mm)" = 154.9). This will keep your previous beam center and detector tilt calibration valid.

In the "General" tab in the Datasets window, choose a "Computation range" from 11° to 22° (**Part I.9**) in order to include the three prominent diffraction peaks (111), (200) and (220) of magnesiowuestite (Fig. 9, 10).

14. View the spectra in "Plot" and "Plot 2D" displays. In the "Plot" display the magnesiowuestite peak at ≈14.3 Å is strangely distorted and in the "Plot 2D" display, it is evident that this distortion is due to one excessively intensive peak in diffraction spectra #64 and #65. This is the diffraction peak from the diamond anvil (Fig. 2b). Remove this spectrum ("Edit" the dataset, and in "Datafiles", select spectrum #64 (this number is indicated in brackets after the datafile name) and click "Remove". Do the same for the spectrum #65. Alternatively these files could be kept in the analysis but not used in the refinement by unchecking the "Enabled" box in the same window. Some spectra may be much weaker (e.g., they are shielded by the beamstop). These could also be removed from the analysis or disabled.

15. Setting up the background in rDAC experiments can be difficult due to scattering and absorption from gaskets and DAC absorption effects (Fig. 2c, 9, 10). In this case it is best to use interpolated backgrounds. This is done by editing the "Dataset" and going to "Background function". Remove all parameters for the "Polynomial" function (select parameter in the panel and click "remove parameter"), then go to the "Interpolated" tab. Check the "Interpolated background" option and enter 10 in the "Points for interpolation" field. Next click "Set interpolation points manually". A diffraction spectrum will appear in a new window. Select "Tools → Edit interpolated background points". A set of 10 automatically created points will be displayed. Some points lie in between peaks, corresponding to the "true" background, but some are located on diffraction peaks. Right-click on a position on the spectrum and select "add" or "remove" from the drop-down menu, in order to add or remove interpolated background points. All background points should be added where intensity is minimal (Fig. 10). Warning: in some

Microsoft Windows and OSX systems and computers with nVidia graphic cards, display of the points may not work correctly. Close the window and reopen it to see the interpolated background points. You may need to repeat the interpolated background setup several times, until all the points are well located.

16. Next load the appropriate phase using a provided structure file (MgFeO.cif). MgFeO.cif is a magnesiowuestite with 10% Fe substituting for Mg, which is specified in atom site occupancies. Calculate model spectra with the "Calculator" button on the toolbar and review the experimental and calculated diffraction patterns (Fig. 9a). Due to the high pressure applied, experimental diffraction peaks are shifted toward higher 2θ values.

17. *Sample*. With only one image and three diffraction peaks, the coverage is largely insufficient to refine the ODF. But in this DAC experiment texture should have axial symmetry around the compression direction. In MAUD, imposing axial symmetry of strain and texture requires the symmetry axis to be perpendicular to MAUD reference pole figure plane. Edit "Sample" in the MAUD main window and in "Sample position" tab set the Chi value to 90°. This will bring the compression direction into the center of the MAUD reference pole figure. The coverage (after this rotation) is shown in Figure 8d. First the compression axis is at A and after the Chi rotation it is at B.

18. Once the instrument, data files, and phase information are loaded, you will need to manually adjust several parameters to get a closer fit to the data before MAUD can run refinements.

- *Intensity*. Adjust the incident intensity ("_pd_proc_intensity_incident" parameter) until it is close to the data (**Part I.12** and **I.18**).
- *Backgrounds*. If using polynomial backgrounds, adjust the first global background coefficient: "_riet_par_background_pol0" parameter (located in the parameters list just above the intensity parameter) until the background intensity is close. If you are using interpolated backgrounds like suggested in (**15**), skip this step.
- *Unit cell parameters*. Since these experiments are at high pressure, you need to decrease the cell parameter "_cell_length_a" (sections **Part I.12** and **I.17**) until the calculated peak positions roughly correspond to observed peaks.

- *Crystallite size and isotropic microstrain*. Adjust the crystallite size "_riet_par_cryst_size" and microstrain "_riet_par_rs_microstrain" until peak width fits (**Part I.9**). Take into account that in the "Plot" display, broadening of peaks is partially due to peak position variations. In this case good starting estimates for crystallite size and microstrain are 300Å and 0.002, respectively.

C. Stress models

19. *Macrostress.* Lattice strain is due to the imposed anisotropic elastic stress and the elastic properties of the crystal. It is exhibited as sinusoidal oscillations in peak position with azimuth. An example of sinusoidal variations with azimuth can be seen in the "Plot 2D" display at the bottom of Fig. 9a. At this point the calculated fit has no dependence of peak position on azimuth because anisotropic stress has not yet been considered in the model. For radial DAC data with anisotropic stress, check the "Plot 2D" display for a good fit for elastic stress rather than the "Plot" display. The "Plot" display shows an average over all spectra, making peaks appear broader due to angle-dependent lattice strain.

There are four models in MAUD that can be used to fit lattice strains, resulting in diffraction peak shifts Two are "stress models" that convert lattice strains to macroscopic stress tensor components, using provided elastic properties of the material. The other two models fit lattice strain distributions and leave it up to the user to calculate stresses by hand.

In axial compression experiments in the DAC, the anvils impose both hydrostatic stresses (pressure) and differential stresses. The symmetric stress tensor σ_{ij} can be separated into hydrostatic σ_p and differential stress D_{ij} components such that:

$$\sigma_{ij} = \begin{bmatrix} \sigma_p & 0 & 0 \\ 0 & \sigma_p & 0 \\ 0 & 0 & \sigma_p \end{bmatrix} + \begin{bmatrix} -t/3 & 0 & 0 \\ 0 & -t/3 & 0 \\ 0 & 0 & 2t/3 \end{bmatrix} = \sigma_p + D_{ij}$$

where t is the axial stress component and provides lower bounds for the yield strength of the material (Singh, 1993; Singh *et al*., 1998). Thus, during refinement of the stresses, the differential stresses should be constrained such that $\sigma_{11} = \sigma_{22}$ and $\sigma_{33} = -2\sigma_{11}$, where σ_{33} is the largest principal stress in the compression direction and is negative (corresponding to

compression), according to the conventions in MAUD. For the analysis described here only deviatoric stresses will be fit with the stress model. Hydrostatic stresses are accounted for by refining unit cell parameters, which in turn can be converted to pressure by utilizing an appropriate equation of state (see below). The reason for treating these separately is that differential stresses will be calculated assuming a linear stress-strain relationship which is only applicable for small strains. The volume changes of the unit cell due to pressure effects are significantly larger than those due to differential stress, and it is best to use an equation of state which properly accounts for the nonlinearity of stress-strain dependence at larger compressions. On the other hand, for the analysis of the residual stresses, *e.g.*, in engineering materials, where stress tensor components values are often within a 0.5 GPa range, it is appropriate to keep initial lattice parameters fixed. One should then only fit either stress or strain values.

To set up a stress model, select the phase from the "Phases" tab in MAUD main window and edit it. In "Advanced models" select one of the following models from the drop-down list in the "Strain" section: 1) "Triaxial Stress Isotropic E", 2) "Moment Pole Stress", 3) WSODF Popa-Balzar, or 4) "Radial Diffraction in the DAC".

We will briefly describe each model and how to set it up for the refinement.

20. *Triaxial Stress Isotropic E.* This model assumes an isotropic material and as a result generally does a poor job of fitting stresses in textured material with pronounced single-crystal elastic anisotropy. But fairly isotropic materials (*e.g.*, zirconium) can be described with it and it can be applied for materials where single crystal elastic properties are unknown and you are not concerned about precise determination of stresses and want to fit textures only.

- Once you have selected "Triaxial Stress Isotropic E" click the "Options" button next to it.
- Enter the Young's modulus and Poisson ratio for the material being analyzed. To obtain an accurate estimate of stresses, you will need to use the Young's modulus and Poisson ratio derived at actual high pressure value.
- Fix the macrostresses with $\sigma_{ij} = 0$ for $i \neq j$, $\sigma_{11} = \sigma_{22}$, and $\sigma_{33} = -2\sigma_{11}$. To fix parameters, right click on the "Macrostress22" value and select "Equal to" from the drop-down menu. This will open the "Parameter binding" window. Scroll down until you find a parameter named "_rista_macrostress_11" for your current phase and select it from the list (in this case with only one phase, it should be near the very end of the parameter list). Enter 1 in

the "x" box, and 0 in the "+" box. This means that "Macrostress22" will be set to 1 * x, "Macrostress11" + 0. Set "Macrostress33" equal to (-2) times "Macrostress11". Now that the stress interdependencies are set, adjust or refine only "Macrostress11". All other stress values will be adjusted automatically.

- Next, manually adjust "Macrostress11" until the sinusoidal variation in peak position in the calculated spectra is close to variations in the observed spectra in the "Plot 2D" display. Generally the off-axis compressive stress should be less than on-axis, thus the 11 differential stress components should be positive.

21. *Moment Pole Stress.* This model is based on (Matthies *et al*., 2001) and requires the elastic tensor (C_{ij}), corrected for pressure, for the material of interest (Figure 11). This is the most sophisticated model of the four. It calculates diffraction elastic constants for each diffraction peak of the material, taking preferred orientation into account, using different micromechanical models similar to those used for calculating bulk polycrystal properties (*i.e.*, Voigt, Reuss, Hill, GEO). The only difference is that for calculation of diffraction elastic constants crystal properties should be averaged, using "moments" of ODF or pole figures (corresponding values weighted by sine or cosine values of certain angles).

- Once you have selected the "Moment Pole Stress" model, click the "Options" button to open the "Moment pole figures options panel".
- Fix the macrostresses as described above with $\sigma_{ij} = 0$ for $i \neq j$, $\sigma_{11} = \sigma_{22}$, and $\sigma_{33} = -2\sigma_{11}$. Again you will only adjust or refine "Macrostress11".
- Enter the single crystal stiffnesses (C_{ij}, in two-index Voigt notation) for the material of interest. Note that the elastic tensor is in general pressure-dependent, and it is important to enter correct values for the given pressure, or the stresses obtained from the model will be incorrect.
- In the "Stress/strain model" box in the top right choose the desired stress model. Voigt, Reuss, Hill, PathGEO, and BulkPathGEO are available. If you choose the Hill model you can adjust the "Weight (Voigt-Reuss)" value to get resulting arithmetically averaged elastic constants closer to either Voigt or Reuss boundary. In almost all cases the BulkPathGEO model is preferable. It satisfies a physically grounded "inversion relation" (i.e., stiffness is inverse compliance) for each aggregate of grains contributing to a

diffraction peak and also for the sample on the macroscopic scale (the latter is not true for the simpler PathGEO model).

- You can include the effects of texture by checking the "Use texture ODF" box. In fact, you are strongly advised to always do so, since differently oriented crystallites are deformed differently by the mean stress field, and their deformation in general depends on elastic constants of the material and thus on the texture. Texture effects will only be accounted for if the "E-WIMV" model is used for the texture description.
- Adjust the "Macrostress11" value until the sinusoidal variation in peak position resembles the data.

22. *WSODF Popa-Balzar*. The model, described in (Popa and Balzar, 2001), in its MAUD implementation does not provide the macrostress tensor components directly. It introduces an orientation distribution function for each strain (and consequently, stress) tensor component that is weighted according to ODF values. So, in addition to the crystal ODF, there are generally six weighted strain ODFs (WSODFs). These WSODFs are expressed as series expansions using spherical harmonics. This method is the least user-friendly, and an inexperienced user may find it very difficult to adjust all the values manually. Thus we give only a short outline of it.

- Once you have selected the "WSODF Popa-Balzar" model click the "Options" button next to it. This will open the "Harmonic strain options panel".
- Select "fiber" as the "Sample symmetry". You can control the length of the series expansion with the slider bar; it should be at least 4. Since this DAC experiment is believed to be centrosymmetric, all the off-diagonal strain components should be set to zero and not refined.
- After the series expansion coefficients are refined, macrostrain can be calculated by clicking the "Compute macrostrain" button (coefficients will appear in a console window). Strain distributions in the sample may be plotted as pole figures (in the MAUD main window, select "Graphic → Texture plot" and "Plot" the "Reconstructed strain"). The macrostress tensor may be calculated with a micromechanical model.

23. *Radial Diffraction in the DAC*. This model is also not a true "stress" model. While previous models can be applied to more complicated deformation geometries, "Radial Diffraction in the

DAC" can only be applied to axial compression. The main advantage of this model is that it allows the user to fit lattice strains for each peak separately whereas previous models imply that all the displacements of diffraction peaks correspond to one macrostress tensor, or they are restricted by crystal symmetry. The "Triaxial Stress Isotropic E" and "Moment Pole Stress" models may fail if plastic anisotropy of the material is high. In the case of magnesiowuestite some peaks exhibit much higher lattice strains than other peaks, and these two models may not be able to provide a satisfactory fit to the data.

The "Radial Diffraction in the DAC" model is built on the model of Singh (1993) and Singh *et al*. (1998). This model fits a *Q*(hkl) factor to each diffraction peak based on peak displacement and the angle to the principal stress axis.

- If you have selected the "Radial Diffraction in the DAC" model, click the "Options" button. This will open the "DAC radial diffraction options panel" (Fig. 12).
- The first two boxes are titled "Alpha" and "Beta". "Beta" is the angle between the sample *Z*-axis and the maximum stress direction. "Alpha" is a rotation around *Z*. These two angles allow you to refine the orientation of the maximum stress axis in case it deviates from the sample *Z*-axis. This does happen fairly frequently at high pressures as the tips of diamond anvils deform elastically and become cupped. For now we will leave these set to zero.
- The following boxes titled "*Q*(hkl)" are the *Q*(hkl) factor for each lattice plane given in the parentheses. *Q*(hkl) should be positive and generally falls in the range of 0.001 to 0.007. A good initial estimate is 0.003. Enter it for the three peaks (111), (200) and (220) in the refinement range.
- Manually adjust each *Q*(hkl) until the lattice strains in the model are close to the observed data.

24. *Checking Sample Orientation.* If the stresses appear to be inverted, *i.e.*, "Macrostress11" or *Q*(hkl) values are negative or the sinusoidal variations in peak positions are offset from the data by 90º (azimuth), then likely the sample orientation is wrong. Check that all the angles for each spectrum, dataset and whole sample correspond to experimental geometry. To check angles for individual spectra in a dataset, edit the dataset in the MAUD main window. Click on the "Datafiles" tab and ensure that angles under "Selected spectrum options" in the "Datafiles" tab

are set properly. To check sample orientation, edit the "Sample" in the MAUD main window, click on the "Sample position" tab where sample orientation angles "Omega", "Chi", and "Phi" can be adjusted. An alternative for assignment of certain angles to datafiles, or sample rotation in the "Sample" tab is to rotate the diffraction image in ImageJ when creating the .esg files, *e.g.* by 90°. As we mentioned earlier (**17**), for the refinement the compression axis needs to be in the center of the pole figure.

You can check if the sample orientation is correct by going to "Graphic → Texture plot" in the main MAUD window. Select "Pole figure coverage" and "Plot" it. By disabling and re-enabling different spectra in the current dataset and plotting actual pole figure coverage you may see how different angles and orientations are related. In our case the pole figure coverage is shown in Figure 8d.

25. *Correcting Young's Modulus and Poisson Ratio or C_{ij} to Pressure.* As mentioned above, you must correct the elastic moduli to pressure should you choose to use the "Triaxial Stress Isotropic E" or the "Moment Pole Stress" models. Elastic moduli are pressure dependent and often become larger as pressure increases or may display critical behavior near phase transitions. To correct elastic moduli for pressure, you will need an appropriate equation of state for your sample and a set of elastic moduli either calculated or experimentally determined for a range of pressures for your material. If your experiment is also at high temperature, you will need to correct for this as well and will also need to know the temperature dependence of elastic constants. In addition, you must account for possible anisotropic thermal expansion of the sample.

The easiest way to correct the elastic moduli is to create a spreadsheet which uses an equation of state, such as a 3rd order Birch-Murnaghan equation of state, to calculate pressure from the fitted unit cell parameters. Next, plot each elastic coefficient (*e.g.*, C_{11}, C_{22}, C_{33}, C_{12} etc. or Young's modulus and Poisson's ratio) versus pressure. Once this is done, calculate a best fit line to each of the elastic constants and determine the equation describing the pressure dependence for each constant. This will allow you to extrapolate or interpolate elastic moduli to any reasonable pressure. Often a linear extrapolation will be good enough. Now use the pressure calculated from your unit cell parameters to determine the appropriate value of the elastic moduli using the equations for your best fit lines. You may need to perform several iterations of this

before the unit cell parameter and stress values stabilize. In other word you will need to calculate the pressure from the unit cell parameter, correct the elastic moduli to the pressure, input the corrected elastic moduli, and run the refinement in MAUD. After doing this you may notice that the unit cell parameter has changed. If so you will need to repeat the previous procedure until the unit cell parameter (and the corresponding pressure value) stabilizes.

D. Refinement

26. *Refine Parameters.* We are ready to begin the refinement. The conditions are too complex to use the Wizard, and we will proceed with a mixture of semi-automatic refinement and manual. In the "Parameter list" click "Fix all parameters," and save the analysis in the MAUD main window. Proceed by freeing and refining the parameters in the order listed below. Refine each parameter or parameters until the fit has converged or visibly is not getting better, then move on to the next parameter. After you have refined a parameter, leave it free to refine as you free and refine the next parameter in the list. If your refinement diverges you may have to intervene with manual adjustments.

- *Intensity and backgrounds*. Here we use interpolated backgrounds, so we refine only the intensity. In the "Parameter list" click "Free scale pars" and refine.
- *Unit cell*. In the case of cubic symmetry such as with magneioswuestite, we refine only "_cell_length_a".
- *Texture.* As seen in the "Plot 2D" display the texture is fairly sharp, thus we may refine the texture early. Select the "E-WIMV" texture model for MgFeO. In the "E-WIMV options panel" select 10 iterations for the texture refinement using the slider bar and a 5° resolution. For "Generate symmetry" start with "none". Once a sample orientation and a texture that is compatible with axial symmetry is verified with pole figure plots (Fig 13a), "cylindrical" sample symmetry should be imposed (Fig. 13b). This greatly improves the effective pole figure coverage.
- *Crystallite size and r.m.s. microstrain*. Here we assume isotropic crystallite size and microstrain. In the "Parameter list" click the "Free microstructure" button and refine. As mentioned earlier, with the coarse-grained LaB_6 standard it is difficult to refine the instrument peak shape, and thus refined crystallite size and microstrain of

magnesiowuestite would not be accurate. Be aware that a negative crystallite size is physically meaningless and indicates that your calibration is wrong.

- *Stress model*. For "Moment pole stress" enter the elastic tensor components for your model. For magnesiowuestite at atmospheric pressure these are $C_{11} = C_{22} = C_{33} = 279.5$ GPa, $C_{12} = C_{13} = C_{23} = 102.2$ GPa, $C_{44} = C_{55} = C_{66} = 142$ GPa, all others are zero (Marquardt *et al*., 2009). For "Triaxial Stress Isotropic E" our starting estimation of Young's modulus is 290 GPa, and of Poisson ratio is 0.2. Either free "Macrostress11" if you used the "Triaxial Stress Isotropic E" or the "Moment Pole Stress" models or free the *Q*(hkl) factors of all the peaks in the refinement range if you used the "Radial Diffraction in the DAC" model (see discussion on model selection and parameters binding for all these models in steps **20-23**). For the "Radial Diffraction in the DAC" model, some values of *Q*(hkl) may diverge during refinement if these peaks are of weak intensity or are not well resolved due to peak overlaps. If this happens you need to fix the appropriate *Q*(hkl) parameter to a reasonable value, or just exclude this peak from the refinement.
- Cell parameters and elastic constants should correspond to the same pressure. Once the stress model has converged, use the unit cell parameters to recalibrate pressure. If using the "Triaxial Stress Isotropic E" or "Moment Pole Stress" models, correct the Young's modulus and Poisson ratio or the C_{ij}s, to the new result for pressure and refine the stresses again. Repeat this process until the stresses and unit cell parameters correspond to the same pressure. You may also do the initial refinement with "Radial Diffraction in the DAC" model. Then, once cell parameters (and thus pressure) are confirmed, you may switch to the "Moment pole stress" model and enter the pressure-corrected C_{ij}s (use Table 2 from Marquardt *et al*., 2009 to estimate pressure from the cell parameter value and their Table 3 to get C_{ij} values for this pressure). Comparison of our refinement results at this point with the equation of state (Marquardt *et al*., 2009), suggests that our pressure value is close to 34.3 GPa (refined cell parameter is ≈ 4.008 Å and corresponding volume is ≈ 64.38 $Å^3$). Thus appropriate the C_{ij} values that should be used for the determination of anisotropic elastic stress tensor are $C_{11} = C_{22} = C_{33} = 578.3$ GPa, $C_{12} = C_{13} = C_{23} = 161.9$ GPa, $C_{44} = C_{55} = C_{66} = 141.4$ GPa, and all others are zero.
- *Thermal factors*. Click "Bound B factors" button in the parameter list to refine them all to the same value. With our limited 2θ region we cannot refine these realistically; they will

serve only as an additional correction parameter to overall peak intensities. Click "Bound B factors" and refine.

- *Beam center*. If your stresses are not fitting well and you observe variations of peak position with angle eta, refine the beam center since it may have changed during DAC positioning. After refining, fix the beam center before continuing with the refinement.
- If there is evidence that the compression direction is tilted, then you may correct for this. If using the "Radial Diffraction in the DAC" model, refine the "Alpha" and "Beta" angles for a better fit. If using the "Triaxial Stress Isotropic E" or the "Moment Pole Stress" models, you may refine the sample orientation angles in "Sample" (refer to step **17**) to bring the compression axis normal to the MAUD reference pole figure projection (corresponding to the sample Z axis). After refinement, fix these before continuing.To improve the fit further, you may also refine the occupation of oxygen atoms (as (Mg,Fe)O could be non-stoichiometric).

27. *Heterogeneities of strain in the DAC cell.* In the "Plot 2D" display you may observe asymmetry between the lower and the upper half of the measured spectra display, while refined spectra demonstrate perfect symmetry. This may be due to heterogeneities of the sample in the DAC, *e.g.* some grains on the periphery of the cell are subjected to lower pressures and deviatoric stress. To accommodate this, use only one half of the diffraction image. Since we imposed axial symmetry of texture and stress state, the entire diffraction pattern is not needed to derive a reasonably accurate ODF. For this case, you may remove, *e.g.*, spectra #36-71 from the analysis (refer to procedure for removing spectra in **5** and **14**) and repeat your refinement.

28. At the end of the refinement the refined cell parameter is 4.0103 (1) Å and the corresponding volume is ≈ 64.48 $Å^3$. For radial diffraction the lattice parameter represents the strain resulting from the hydrostatic (pressure) component of the stress tensor. The derived pressure is ≈ 33.9 GPa and the elastic tensor $C_{11} = C_{22} = C_{33} \approx 574.8$ GPa, $C_{12} = C_{13} = C_{23} \approx 161.2$ GPa, $C_{44} = C_{55} = C_{66} \approx 141.7$ GPa; the differential macrostress 11 component is ≈ 1.26 GPa.

In this analysis we have been mainly concerned with preferred orientation which is displayed as pole figures (Fig. 13a,b). For materials with fiber symmetry inverse pole figures that represent the probability of the fiber axis relative to crystal coordinates is an efficient way to

represent textures. Figure 13c is the inverse pole figure of the compression direction plotted in MAUD and Figure 13d the inverse pole figure after processing with BEARTEX. The texture is rather sharp with a pole density maximum of ≈ 11.5 multiples of a random distribution, located close to 001 (Fig. 13d), as observed previously (*e.g.*, Merkel *et al*., 2002; Lin *et al*., 2009).

IV. CONCLUSIONS

Synchrotron X-rays provide a powerful method for quantitative texture analysis of materials. Depending on sample size, beam size and wavelength, small (< 100 μm^3) to large volumes (> 200 mm^3) can be analyzed, and different sample equipment can be used to impose different conditions on the sample (*e.g.*, high pressure, high temperature, anisotropic stress). Compared to neutron diffraction, electron backscatter diffraction or pole-figure goniometry, data acquisition is fast, but data analysis is non-trivial. For complex polyphase materials (such as the shale sample) a careful manual procedure is necessary. Further complications arise for high pressure experiments, where anisotropic stresses need to be accounted for. MAUD incorporates a set of methods able to account for preferred orientations, anisotropic stresses and microstructural characteristics of material. Here we provided only a brief overview of these and simplified step-by-step procedures that give general directions for the analysis, while highlighting some possible complications. Knowledge of the instrument, sample, and experimental setup is necessary to adjust these procedures to each specific case and obtain convincing results.

Acknowledgements

This project was supported by NSF (EAR-0836402) and DOE (DE-FG02-05ER15637). We greatly appreciate access to beamline 11-ID-C at APS of Argonne National Laboratory and help from Chris Benmore and Yang Ren, as well as access to beamline 12.2.2. at ALS of Lawrence Berkeley Laboratory and haelp from Jason Knight. The tutorial was developed as part of a workshop at the Advanced Light Source in fall 2012, supported by CDAC, APS (BESSRC), NSF-COMPRES, ALS and STONE-LANL. RV appreciates support of AYSS JINR (12-401-01).

References

Bish, D.L., and Von Dreele, R.B. (**1989**). "Rietveld refinement of non-hydrogen atomic positions in kaolinite," Clays and Clay Minerals **37**, 289-296.

Gualtieri, A.F. (**2000**). "Accuracy of XRPD QPA using the combined Rietveld-RIR method," Journal of Applied Crystallography **33**, 267-278.

Hammersley, A.P. (**1998**) Fit2D: V99.129 Reference Manual Version 3.1. Internal Report ESRF – 98 – HA01.

Hornby, B.E. **(1998)**. "Experimental laboratory determination of the dynamic elastic properties of wet, drained shales," Journal of Geophysical Research **103** (B12), 29945-29964.

Kaercher, P., Speziale, S., Miyagi, L., Kanitpanyacharoen, W., and Wenk, H.-R. **(2012)**. "Crystallographic preferred orientation in wüstite (FeO) through the cubic-to-rhombohedral phase transition," Physics and Chemistry of Minerals **39**, 613-626.

Kanitpanyacharoen, W., Merkel, S., Miyagi, L., Kaercher, P., Tomé, C.N., Wang, Y., and Wenk, H.-R. **(2012b)**. "Significance of mechanical twinning in hexagonal metals at high pressure," Acta Materialia **60**, 430-442.

Kanitpanyacharoen, W., Wenk, H.-R., Kets, F., Lehr, B.C., and Wirth, R. **(2011)**. "Texture and anisotropy analysis of Qusaiba shales," Geophysical Prospecting **59**, 536-556.

Kanitpanyacharoen, W., Kets, F.B., Wenk, H.-R., and Wirth, R. **(2012a)**. "Mineral preferred orientation and microstructure in the Posidonia Shale in relation to different degrees of thermal maturity," Clays and Clay Minerals **60**, 315-329.

Kunz, M., Caldwell, W.A., Miyagi, L., and Wenk, H.-R. **(2007)**. "In situ laser heating and radial synchrotron x-ray diffraction in a diamond anvil cell," Review of Scientific Instruments **78**, 063907, 1-6.

Lin J.-F., Wenk H.-R., Voltolini, M., Speziale S., Shu J., and Duffy T. **(2009)**. "Deformation of lower mantle ferropericlase (Mg,Fe)O across the electronic spin transition," Phys. Chem. Minerals **37**, 585-592.

Lutterotti, L., Matthies, S., Wenk, H.-R., Schultz, A.S., and Richardson, J.W. (**1997**). "Combined texture and structure analysis of deformed limestone from time-of-flight neutron diffraction spectra," Journal of Applied Physics **81**, 594-600.

Lutterotti, L., Voltolini, M., Wenk, H.-R., Bandyopadhyay, K., and Vanorio, T. (**2010**). "Texture analysis of turbostratically disordered Ca-montmorillonite," American Mineralogist **95**, 98-103.

Marquardt, H., Speziale, S., Reichmann, H.J., Frost, D.J., and Schilling, F. R. **(2009)**. "Single-crystal elasticity of $(Mg_{0.9}Fe_{0.1})O$ to 81 GPa," Earth and Planetary Science Letters **287**, 345-352.

Matthies, S., and Wenk, H.-R **(2009)**. "Transformations for monoclinic crystal symmetry in texture analysis," Journal of Applied Crystallography **42**, 564-571.

Matthies, S., Priesmeyer, H.G., and Daymond, M.R. **(2001)**. "On the diffractive determination of single-crystal elastic constants using polycrystalline samples," Journal of Applied Crystallography **34**, 585-601.

Merkel, S., Wenk, H.-R., Shu, J., Shen, G., Gillet, P., Mao, H.-K., and Hemley, R.J. **(2002)**. "Deformation of polycrystalline MgO at pressures of the lower mantle," Journal of Geophysical Research **107** doi:10.1029/2001JB000920, 1-17.

Merkel, S. **(2006)**. "X-ray diffraction evaluation of stress in high pressure deformation experiments," Journal of Physics: Condensed Matter **18**, S949-962.

Miyagi, L., Kanitpanyacharoen, W., Kaercher, P., Lee, K.K.M., and Wenk, H.-R. **(2010)**. "Slip systems in $MgSiO_3$ post-perovskite: Implications for D'' anisotropy," Science **329**, 1639-1641.

Miyagi, L., Kunz, M., Knight, J., Nasiatka, J., Voltolini, M., and Wenk, H.-R. **(2008)**. "*In situ* phase transformation and deformation of iron at high pressure and temperature," Journal of Applied Physics **104**, 103510, 1-9.

Miyagi. L., Kanitpanyacharoen. W., Kaercher. P., Knight. J., Raju. V., Zepeda. E., Wenk. H.R., and Williams. Q. **(2013)**. "Combined resistive and laser heating in diamond anvil high pressure experiments". Rev. Sci. Instr. (in press)

Plançon A., Tsipurski S.I., and Drits V.A. **(1985)**. "Calculation of intensity distribution in the case of oblique texture electron diffraction," Journal of Applied Crystallography **18**, 191-196.

Popa, N.C., and Balzar, D. (**2001**). "Elastic strain and stress determination by Rietveld refinement: generalized treatment for textured polycrystals for all Laue classes," Journal of Applied Crystallography **34**, 187-195.

Singh, A.K. **(1993)**. "The lattice strains in a specimen (cubic system) compressed nonhydrostatically in an opposed anvil device," Journal of Applied Physics 73, 4278-4286.

Singh, A.K., Mao, H.-K., Shu, J., and Hemley, R.J. **(1998)**. "Estimation of single-crystal elastic moduli from polycrystalline X-ray diffraction at high pressure: application to FeO and iron," Physical Review Letters **80**, 2157-2160.

Ufer, K., Roth, G., Kleeberg, R., Stanjek, H., Dohrmann, R., and Bergmann, J. **(2004)**. "Description of X-ray powder pattern of turbostratically disordered layer structures with a Rietveld compatible approach," Zeitschrift für Kristallographie **219**, 519-527.

Vasin, R., Wenk, H.-R., Kanitpanyacharoen, W., Matthies, S., and Wirth, R. **(2013)**. "Anisotropy of Kimmeridge shale," J. Geophys. Res. (submitted).

Wenk, H.-R., Lonardelli, I., Merkel, S., Miyagi, L., Pehl, J., Speziale, S., and Tommaseo, C.E. **(2006)**. "Deformation textures produced in diamond anvil experiments, analyzed in radial diffraction geometry," Journal of Physics: Condensed Matter **18**, S933-947.

Wenk, H.-R., Ischia, G., Nishiyama, N., Wang, Y., and Uchida, T. **(2005)**. "Texture development and deformation mechanisms in ringwoodite," Physics of the Earth and Planetary Interiors **152**, 191-199.

Wenk, H.-R., Matthies, S., Donovan, J., and Chateigner, D. (**1998**). "BEARTEX: a Windows-based program system for quantitative texture analysis," Journal of Applied Crystallography **31**, 262-269.

Wenk, H.-R., Vasin, R.N., and Lutterotti, L. **(2013)**. "Rietveld texture analysis from synchrotron diffraction images: I. Basic analysis,". Powder Diffraction (submitted).

Wenk, H.-R., Voltolini, M., Kern, H., Popp, T., and Mazurek, M. **(2008)**. "Anisotropy in shale from Mont Terri," The Leading Edge **27**, 742-748.

Wenk, H.-R., Kanitpanyacharoen, W., and Voltolini, M. **(2010)**. "Preferred orientation of phyllosilicates: Comparison of fault gouge, shale and schist," Journal of Structural Geology **32**, 478-489.

Tables

Table 1 Phase volume and weight fractions of minerals in shale (in %), with and without imposed axial symmetry of texture.

	Vol. Axial	Wgt. Axial	Vol. No symm.	Wgt. No symm.
Kaolinite	6.8	6.2	7.2	6.6
Illite-mica	23.7	23.7	26.2	26.1
Illite-smectite	31.4	29.2	30.5	28.3
Quartz	31.9	29.9	29.9	27.9
Pyrite	6.2	11.0	6.3	11.1

Table 2 Texture information for phyllosilicates in shale after processing in BEARTEX, pole densities in m.r.d.

	Max axial	Min axial	Max No symm.	Min No symm
Kaolinite 001	6.84	0.22	5.14	0.31
Illite-mica 100	8.50	0.12	7.78	0.25
Illite-smectite 100	3.83	0.39	3.70	0.30

Table 3 Texture information for magnesiowuestite after processing data in BEARTEX; pole densities of different pole figures and inverse pole figure (IPF) in m.r.d.

	Max	Min		
001	5.70	0.33		
110	1.59	0.47		
111	2.11	0.12		
IPF	10.74	0.11		

Figure Captions

Figure 1. (a) Slab of shale embedded in epoxy and mounted on a pin. (b) Pole figure coverage with a single image, bedding plane normal is at A. When cylindrical symmetry is imposed bedding plane normal is rotated to B by a chi rotation; each point covers a circle around B on the pole figure (c) Coverage with seven images recorded at different sample tilts omega, (d) after 90º rotation around chi to bring the bedding plane normal into the center.

Figure 2. 2D synchrotron diffraction images. (a) Kimmeridge shale with many phases, some with strong preferred orientation. (b) LaB6 standard, rather coarse-grained and with some impurities. (c) Radial diffraction DAC experiment on magnesiowuestite. Arrow points to a diffraction spot from diamond.

Figure 3. Stack of diffraction spectra for Kimmeridge shale, omega = 0 tilt image. Experimental data at bottom and Rietveld fit on top. Some diffraction lines are labeled.

Figure 4. Window in MAUD to define background peaks.

Figure 5. Two diffraction spectra of Kimmeridge shale with scattering lattice planes parallel to bedding plane on top and perpendicular to it at bottom. Crosses are measured data and line is Rietveld fit. Below the spectra is a list of contributing phases and their corresponding diffraction peak positions are marked with ticks.

Figure 6. Pole figures of basal planes of kaolinite, illite-mica and illite-smectite for Kimmeridge shale. (a) Derived from a single image, imposing fiber symmetry. (b) Result for 7 images without imposing symmetry. The corresponding pole figure coverage is shown in Fig. 1d. Equal area projection on the bedding plane, contours in multiples of a random distribution.

Figure 7. Pole figures 100 of kaolinite and 001 of illite-mica and illite-smectite for Kimmeridge shale without imposing sample symmetry. The corresponding pole figure coverage is shown in

Fig. 1d. Equal area projection on the bedding plane, contours in multiples of a random distribution.

Figure 8. (a,b) Schematic sketch illustrating the geometry of deformation experiments in a diamond anvil cell in radial diffraction geometry. (c) Actual diamond culets compressing a sample contained by a gasket. (d) Pole figure coverage for the magnesiowuestite DAC experiment. A gap is visible where two spectra are disabled because they contain a diffraction spot from the diamond.

Figure 9. Measured (bottom) and calculated (top) diffraction spectra for magnesiowuestite; (a) at the beginning of the refinement. Lattice parameters are wrong and there is no texture or anisotropic stress in the model. Also note the black diffraction spot from diamond. (b) At the end of the refinement there is an excellent match in position, width and intensity. The compression direction is indicated by the arrow in (a) (larger 2θ angle corresponding to smaller d-spacing).

Figure 10. Plot display of diffraction pattern of magnesiowuestite. Dots indicate user-defined positions for background interpolation.

Figure 11. MAUD window for moment pole figures option to use as a stress/strain model.

Figure 12. MAUD radial diffraction option panel for stress-strain refinement.

Figure 13. Texture information for magnesiowuestite at 34 GPa represented as pole figures (a-b) and inverse pole figures (c-d). (a) Pole figures without imposing sample symmetry. (b) Pole figures imposing fiber symmetry. (c) Inverse pole figure of the compression direction plotted by MAUD. (d) Inverse pole figure after processing data in BEARTEX. Equal area projection, contours in multiples of a random distribution.

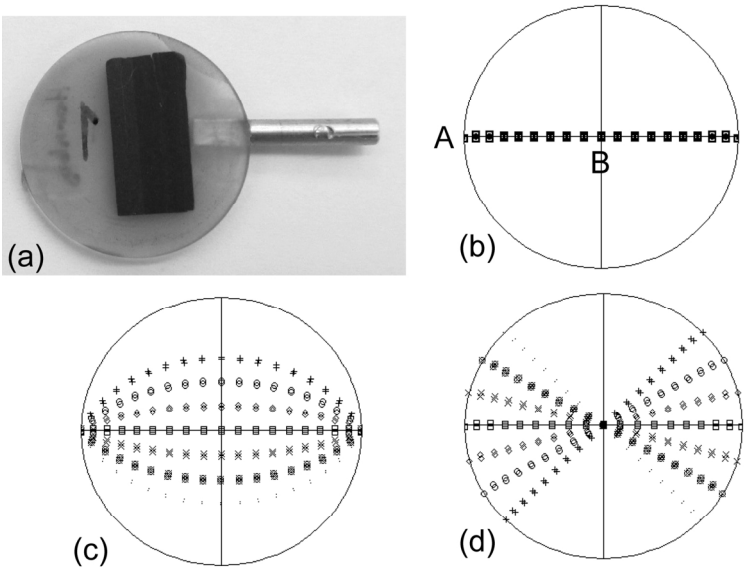

Figure 1. (a) Slab of shale embedded in epoxy and mounted on a pin. (b) Pole figure coverage with a single image, bedding plane normal is at A. When cylindrical symmetry is imposed bedding plane normal is rotated to B by a chi rotation; each point covers a circle around B on the pole figure (c) Coverage with seven images recorded at different sample tilts omega, (d) after 90º rotation around chi to bring the bedding plane normal into the center.
173x107mm (300 x 300 DPI)

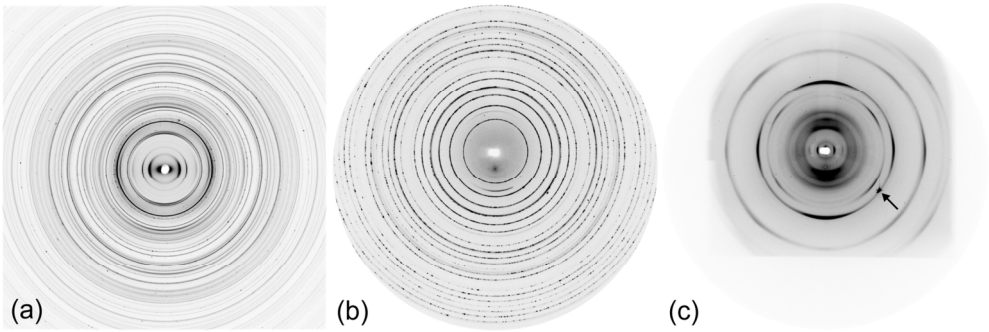

Figure 2. 2D synchrotron diffraction images. (a) Kimmeridge shale with many phases, some with strong preferred orientation. (b) LaB6 standard, rather coarse-grained and with some impurities. (c) Radial diffraction DAC experiment on magnesiowuestite. Arrow points to a diffraction spot from diamond.
147x51mm (300 x 300 DPI)

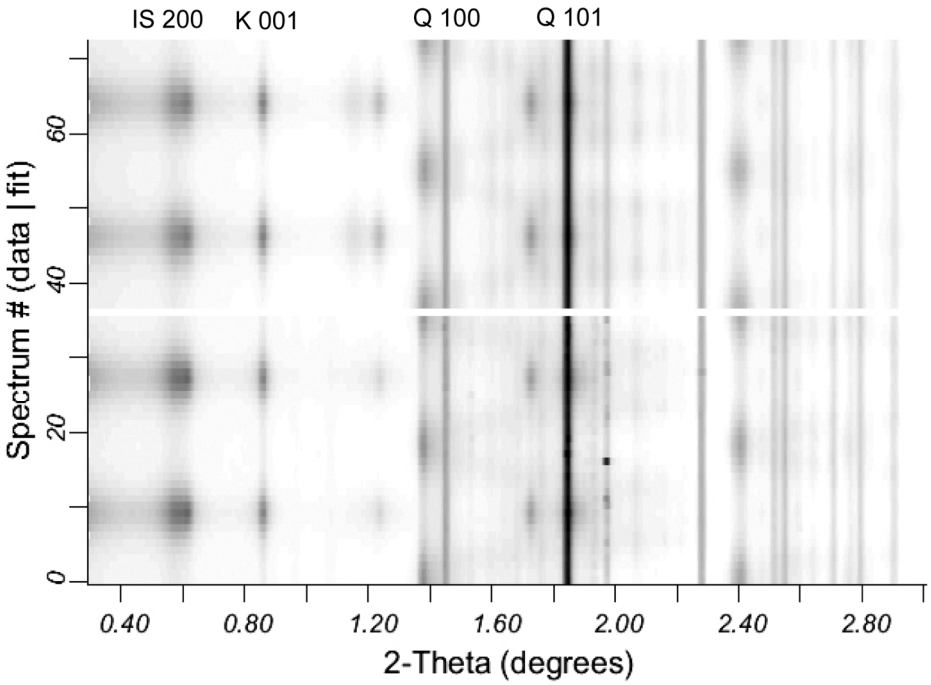

Figure 3. Stack of diffraction spectra for Kimmeridge shale, omega = 0 tilt image. Experimental data at bottom and Rietveld fit on top. Some diffraction lines are labeled.
173x121mm (300 x 300 DPI)

Figure 4. Window in MAUD to define background peaks.
18x12mm (300 x 300 DPI)

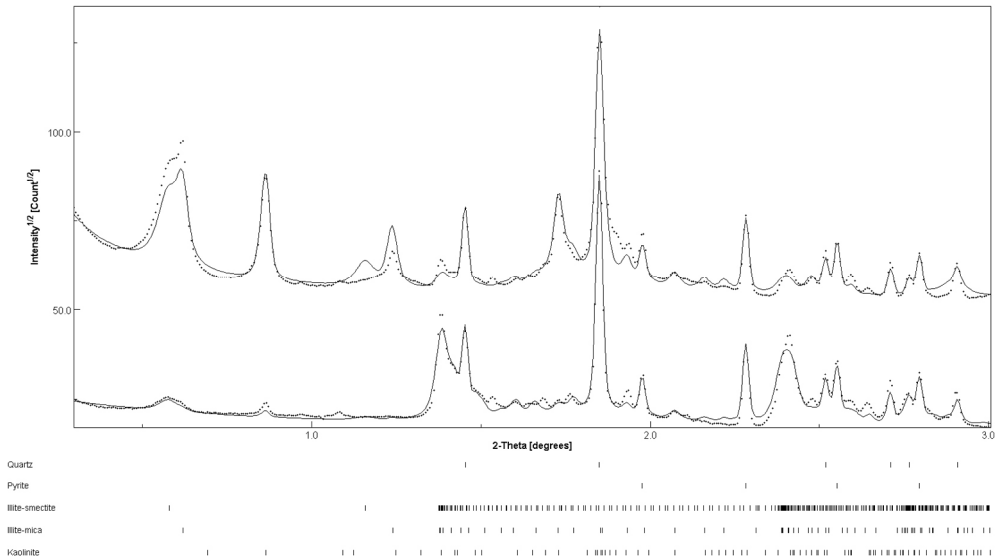

Figure 5. Two diffraction spectra of Kimmeridge shale with scattering lattice planes parallel to bedding plane on top and perpendicular to it at bottom. Crosses are measured data and line is Rietveld fit. Below the spectra is a list of contributing phases and their corresponding diffraction peak positions are marked with ticks.
213x123mm (200 x 200 DPI)

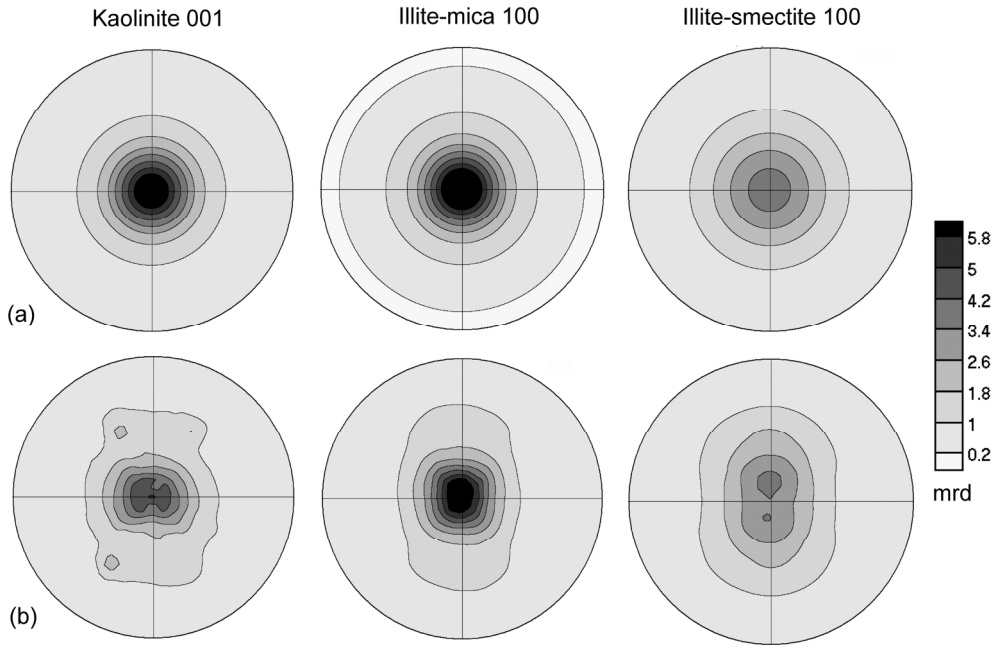

Figure 6. Pole figures of basal planes of kaolinite, illite-mica and illite-smectite for Kimmeridge shale. (a) Derived from a single image, imposing fiber symmetry. (b) Result for 7 images without imposing symmetry. The corresponding pole figure coverage is shown in Fig. 1d. Equal area projection on the bedding plane, contours in multiples of a random distribution.
198x127mm (300 x 300 DPI)

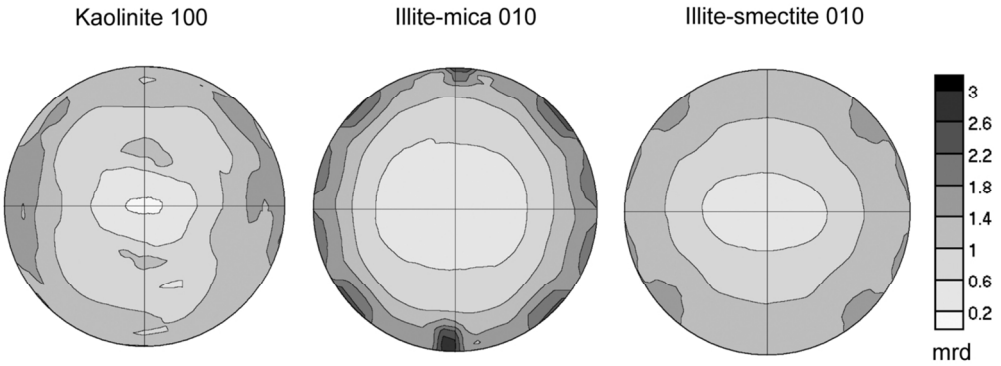

Figure 7. Pole figures 100 of kaolinite and 001 of illite-mica and illite-smectite for Kimmeridge shale without imposing sample symmetry. The corresponding pole figure coverage is shown in Fig. 1d. Equal area projection on the bedding plane, contours in multiples of a random distribution.
114x43mm (300 x 300 DPI)

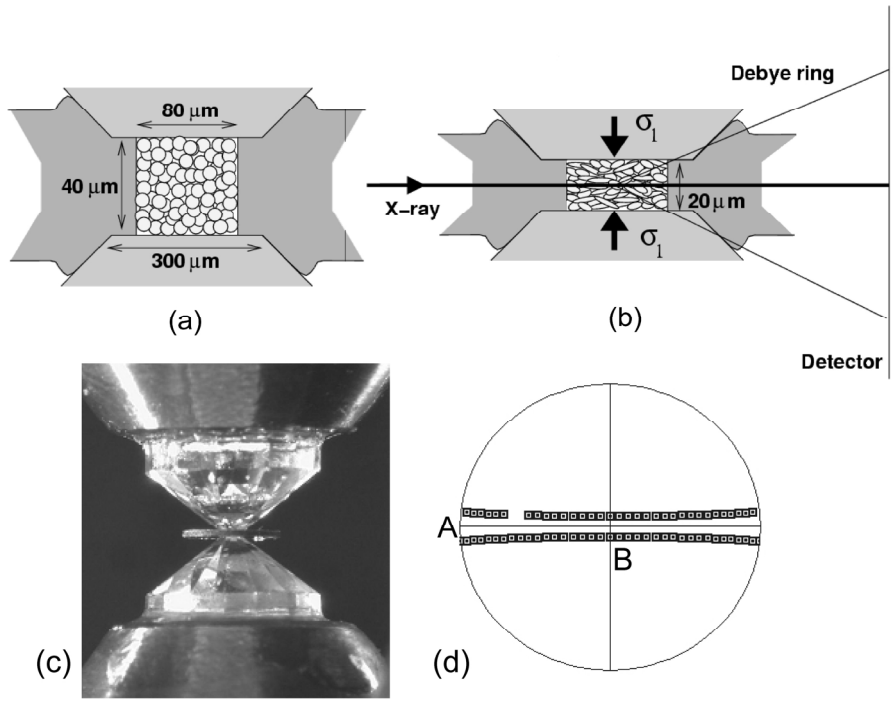

Figure 8. (a,b) Schematic sketch illustrating the geometry of deformation experiments in a diamond anvil cell in radial diffraction geometry. (c) Actual diamond culets compressing a sample contained by a gasket. (d) Pole figure coverage for the magnesiowuestite DAC experiment. A gap is visible where two spectra are disabled because they contain a diffraction spot from the diamond.
199x145mm (300 x 300 DPI)

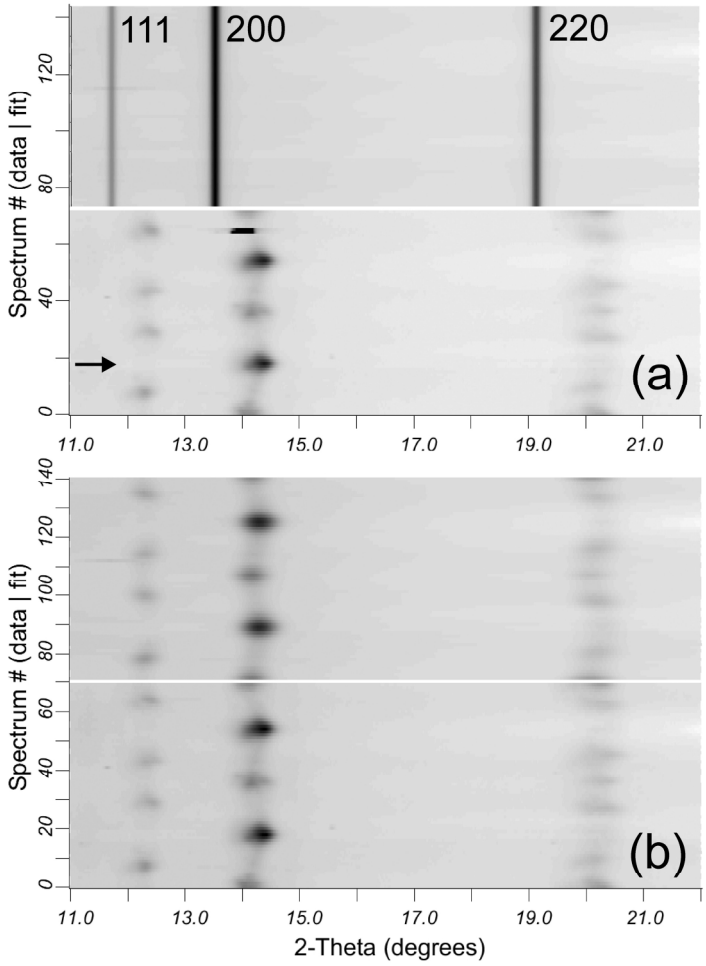

Figure 9. Measured (bottom) and calculated (top) diffraction spectra for magnesiowuestite; (a) at the beginning of the refinement. Lattice parameters are wrong and there is no texture or anisotropic stress in the model. Also note the black diffraction spot from diamond. (b) At the end of the refinement there is an excellent match in position, width and intensity. The compression direction is indicated by the arrow in (a) (larger 2θ angle corresponding to smaller d-spacing).
227x221mm (300 x 300 DPI)

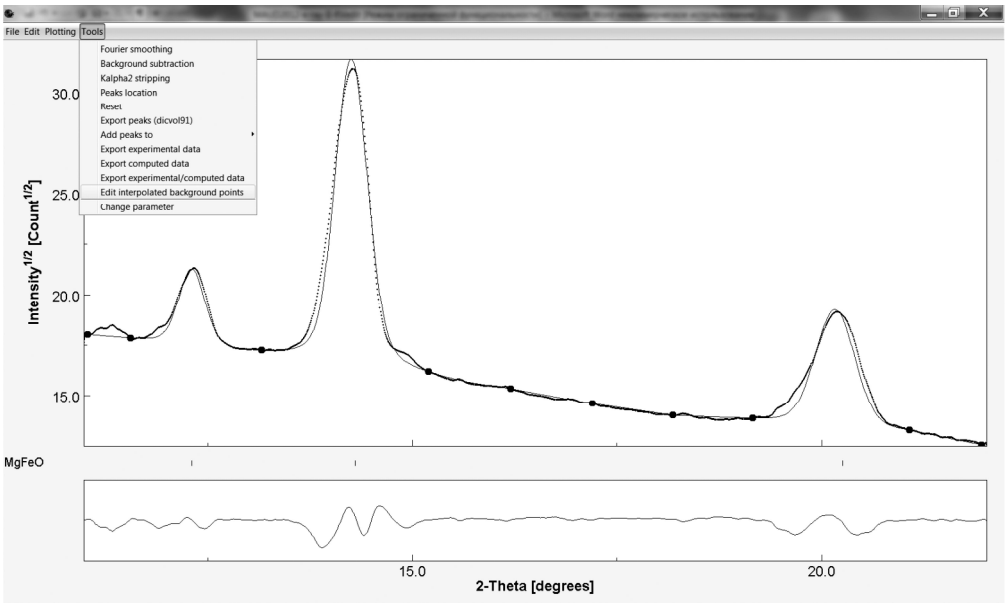

Figure 10. Plot display of diffraction pattern of magnesiowuestite. Dots indicate user-defined positions for background interpolation.
1482x884mm (72 x 72 DPI)

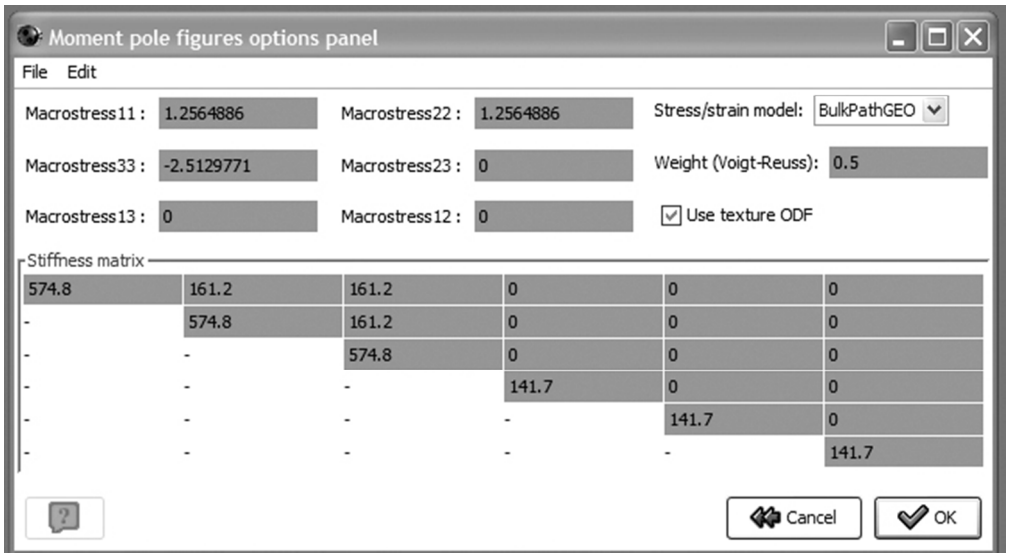

Figure 11. MAUD window for moment pole figures option to use as a stress/strain model.
227x124mm (72 x 72 DPI)

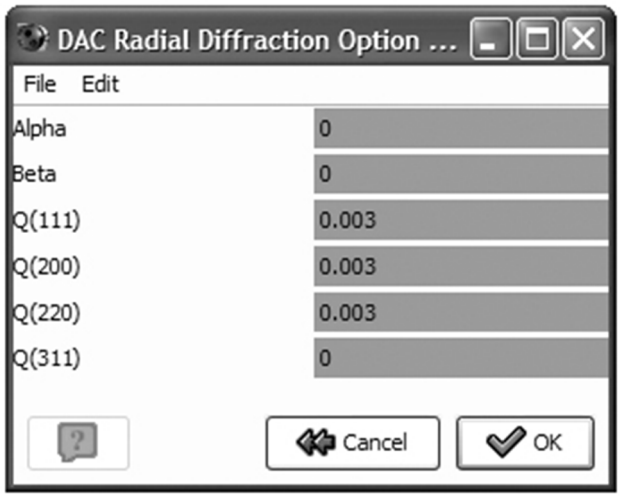

Figure 12. MAUD radial diffraction option panel for stress-strain refinement.
110x87mm (72 x 72 DPI)

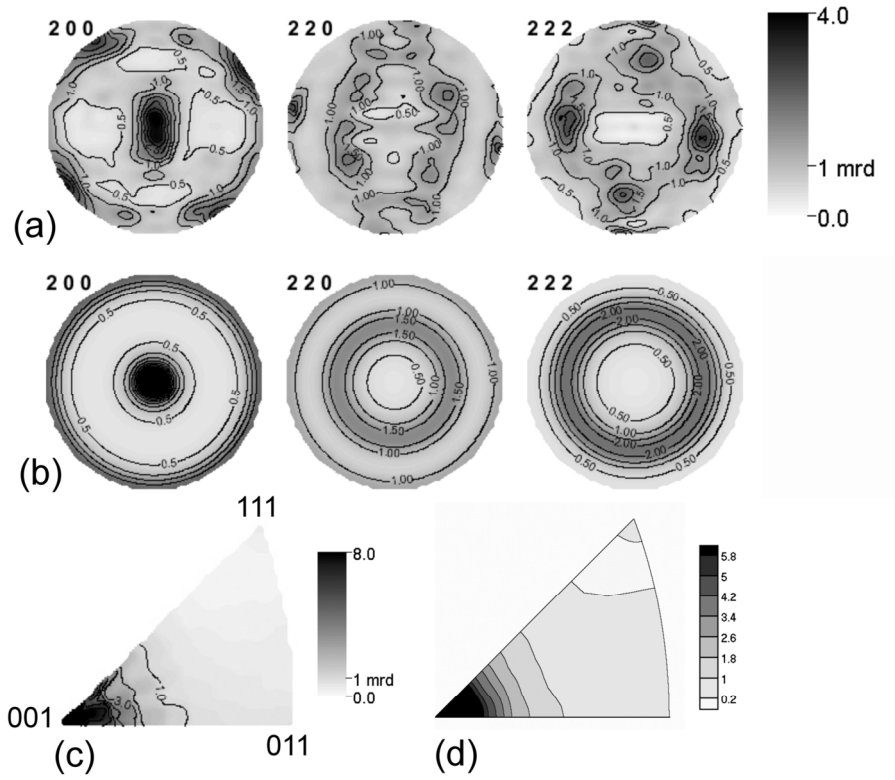

Figure 13. Texture information for magnesiowuestite at 34 GPa represented as pole figures (a-b) and inverse pole figures (c-d). (a) Pole figures without imposing sample symmetry. (b) Pole figures imposing fiber symmetry. (c) Inverse pole figure of the compression direction plotted by MAUD. (d) Inverse pole figure after processing data in BEARTEX. Equal area projection, contours in multiples of a random distribution.
157x126mm (300 x 300 DPI)